Available online at www.sciencedirect.com

ScienceDirect

Procedia Engineering 130 (2015) 652 – 661

Procedia Engineering

www.elsevier.com/locate/procedia

14th International Conference on Pressure Vessel Technology

Nanoindentation Experimental Study on Mechanical Properties of As-cast BNi-2 Solder Alloy

D.Q. Chen[a], G.-Y. Zhou[a,*], Z.P. Liu[a], S.-T. Tu[a]

[a]*Key Laboratory of Pressure Systems and Safety (MOE), East China University of Science and Technology, Shanghai 200237, China*

Abstract

Nanoindentation testing has been used to study mechanical properties of as-cast BNi-2 solder alloy. Hardness and modulus were measured by the nanoindentation experiments. It is confirmed that it is loading rates insensitive to as-cast BNi-2 filler metal from the elasto-plastic nanoindentation responses. In this study, indentation size effect has been discussed. It is found that as-cast BNi-2 is independent of the indentation size effect. Using the model proposed by Dao et al., the yield strength and work hardening exponent were regressed from the loading–unloading behavior during indentation. The purpose of the present work is to obtain a comprehensive elastic–plastic properties understanding of as-cast BNi-2 filler metal which can be better application for engineering.

Peer-review under responsibility of the organizing committee of ICPVT-14

Keywords: BNi-2 solder alloy; mechanical properties; Nanoindentation

1. Introduction

A kind of high temperature alloy BNi-2 has been widely used in mechanical, chemical, aerospace and other fields due to its low melting temperature, good wetting and flow characteristics [1]. With good wetting ability, nickel-based solder and base material have good comprehensive properties of brazed joints. The solders are intended to provide thermal and mechanical continuity to the package and therefore are highly important for the reliability of the system. Significant researches have been focused on the brazing processing and the effect of temperature and clearance on brazing joints [2-5]. In a recent previous work [6], the kinetics and mechanisms of brazing were

* Corresponding author. Tel.: +86-021-64253513; fax: + 86-021-64253513.
E-mail address: zhougy@ecust.edu.cn.

Peer-review under responsibility of the organizing committee of ICPVT-14
doi:10.1016/j.proeng.2015.12.289

determined, as well as the phases involved in the joint formation, in the case of pure nickel brazed with a usual filler alloy called BNi-2. In addition, the residual stress and distortion analysis after brazing and creep-rupture resistance for brazing joint at high temperature have been investigated [7]. Application of such alloys requires a comprehensive understanding of their mechanical properties at small volume size and at elevated temperatures. However, such information is still lacking for both solder joints and bulk alloy.

In real application, the thickness of the BNi-2 filler metal can be in the range of a few microns and the intermetallic compounds of solder joints can be under micron in dimension. Thus, nanoindentation is a suitable tool for these extremely small-scale components. Nanoindetation technique, which has been widely used in characterizing mechanical properties of small-scaled structure without destruction of the samples, provides accurate controls on load, displacement and position. Based on the continuous load-depth curves, a great deal of information about the mechanical properties and deformation of the material beneath the indenter could be obtained [8-10]. For example, the hardness and Young's modulus can be obtained from the maximum load and the initial unloading slope using the methods suggested by Oliver and Pharr [10] or Doerner and Nix [11]. Nanoindentation has also been used to measure Young's modulus and hardness of thin films [12-15], microstructural phases [16-18], and bulk materials [19,20]. Recently, the plastic properties of a material, such as yield stress and work hardening exponent have also been extracted from instrumented indentation [21-24]. It is confirmed that it is a useful tool for evaluating the elastic and plastic properties of materials and components. Damping and internal friction properties such as the storage and loss modulus [25,26], activation energy and stress exponent for creep [8,27], and fracture toughness of brittle materials [28,29] have also been measured using nanoindentation technique. These studies have investigated the mechanical behavior of the component of the solder joint structure, bulk solder in the as-soldered condition and other small-scale structures.

In this study, the mechanical properties of as-cast BNi-2 filler metal were investigated by nanoindentation tests. Nanoindentation has the capability to accurately measure the Young's modulus and hardness of small volumes, which is explored on the cast BNi-2 filler metal in this work. Using the model by Dao et al. [30], the yield strength and work hardening exponent could be extracted from the loading–unloading behavior during indentation.

2. Experimental procedure

BNi-2 was prepared by casting BNi-2 solder powder in a stainless steel vessel. BNi-2 were heated to 1120°C at heating rate of 20°C /min in a vacuum less than 0.02Pa condition, rapid cooling with liquid nitrogen till 1000°C after 15min incubation and 20min heat preservation let the element diffusion homogeneously, then obtained as-cast BNi-2 filler metal along with furnace cooling. Table 1 shows the chemical compositions (in wt%) of the solder used in this study. The as-cast BNi-2 was machined into cubes of 8mm×6mm×3mm, 10mm×10mm×3mm, respectively. The solder was then carefully ground with sand paper down to 800, 1000 and 2000 grit, followed by polishing with 0.5um diamond suspension. The sample was cleaned in ethanol and distilled water and dried immediately.

Table 1. The compsitions of as-cast BNi-2 solder alloy.

Material	Compsition	B	Si	Cr	Fe	Ni
BNi-2	wt %	0.07	4.84	8.03	6.93	80.13

Figure 1 shows the instrumented nanoindentation system (Agilent G200, USA). The maximum load of the machine is 500mN and the load resolution of the system is less than 30nN. The maximum indentation depth of the system is 500um and the displacement resolution is less than 0.001nm. Nanoindentation tests were conducted on the as-cast BNi-2 solder alloy to acquire its mechanical properties. All indentation tests were performed at room temperature. Indentation was conducted with a three-sided pyramid Berkovich indentor on polished samples. Calibration for modulus or hardness can be evaluated as a function of indentation depth [31].

Load-unload experiments were performed to understand the effects of different loading conditions. In order to minimize plastic effects, the indenter was loaded and unloaded twice in a constant loading rate, with which unloading is terminated at 10% of the peak load to assure that contact is maintained between the specimen and the indenter. Loading/unloading rates of 0.5mN/s, 1mN/s, 5mN/s and 10mN/s and the maximum load of 8mN, 35mN

and 65mN, 10s holding time at the peak indentation load were used in the experiment. The depths ranged from 200nm to 700nm. After the last unloading, the load was held constant for a period of 80s at the 10% of the peak value while the displacement was carefully monitored the thermal drift. Young's modulus and hardness values for a given indentation are taken as the average value over a specimen depth where the modulus and hardness were independent of depth, i.e., between approximately 100–700 nm into the specimen. Each test was performed five times measurement and took the average result.

Fig. 1. Instrumented nanoindentation system(Agilent G200, USA).

3. Results and discussions

During a typical nanoindentation test, load and displacement are recorded as the indenter tip is pressed into the test material's surface with a prescribed loading and unloading profile. The response of interest is the load-displacement curve (often called the *P-h* curve) as depicted in Fig. 3 for an indentation on BNi-2.

3.1. Young's modulus and hardness

In this section, we describe the analysis method developed by Oliver and Pharr [10] for obtaining Young's modulus and hardness from the indentation curves, as well as the modulus and hardness results. A typical indentation load–displacement curve for BNi-2 is shown in Fig. 2. The Young's modulus was obtained by first measuring the contact stiffness, *S*. This may be obtained from the slope on unloading, $S=(dP/dh)h_{max}$. The contact stiffness is then related to the reduced Young's modulus, E_r, by the following relation [10]

$$E_r = \frac{\sqrt{\pi}}{2\beta}\frac{S}{\sqrt{A}} \tag{1}$$

where β is a constant that depends on the geometry of the indenter (β= 1.034 for a Berkovich indenter) [31] and A is the projected contact area of indentation. E_r is the reduced elastic modulus, which accounts for the fact that elastic deformation occurs in both the sample and the indenter, can be related to the Young's modulus by:

$$\frac{1}{E_r} = \left(\frac{1-\nu^2}{E}\right) + \left(\frac{1-\nu_i^2}{E_i}\right) \tag{2}$$

where E and ν are the sample Young's modulus and Poisson's ratio, respectively, and the subscript i refers to the indenter. In this study, E_i was taken as 1141 GPa and ν_i as 0.07[9,32].

For an indenter with a known geometry, the projected contact area is a function of the contact depth. The area function for a perfect Berkovich indenter is given by:

$$A_c = 24.56h_c^2 \tag{3}$$

Indenters used in practical nanoindentation testing are not ideally sharp. Therefore, tip geometry calibration or area function calibration is needed. A series of indentations is made on fused quartz at depths of interest. A plot of A_c versus h_c can be curve fit according to the following functional from:

$$A_c = 24.56h_c^2 + \sum_{i=0}^{7} C_i h_i^{\frac{1}{2i}} \tag{4}$$

where C_i are constants when i equals to 0 and 7. The lead term describes a perfect Berkovich indenter, the others describe deviations from the Berkovich geometry due to blunting of the tip [10].

The contact depth can be estimated from the load - displacement data using Eq. (5):

$$h_c = h_{\max} - \varepsilon \frac{P_{\max}}{S} \tag{5}$$

where ε is a constant that depends on the indenter geometry (ε= 0.75 for a Berkovich indenter).

The Young's modulus E is obtained from Eqs. (1) and (2). The hardness of a material is defined as its resistance to plastic deformation. Thus, hardness H is determined from maximum indentation load P_{max} divided by the actual projected contact area A_c and written as:

$$H = \frac{P_{max}}{A_c} \tag{6}$$

Load–displacement responses for filler metal BNi-2 are shown in Fig. 2 which shows a comparison of the results tested in different values of the maximum load and loading rates. It can clearly be observed that the sample exhibits elasto-plastic behaviour at room temperature. Most *P–h* curves with increasing loads coincide well with each other. The curves demonstrate a smooth shape, and no pop-in could be detected. When the loading rate decreased from 10mN/s to 0.5mN/s, the displacement into surface increased slightly which can be seen in Fig. 2 (b). For example, with the same load of 8mN during the increase, the displacement was 216nm when the load rate was 0.5mN/s, while it was 207nm for a load rate of 10mN/s. At the maximum load of 65mN, the difference of displacement could be 16nm between the load rate of 0.5mN/s and 10mN/s. The difference in the different rates during loading causes a small difference in depth. Because of longer time the plastic deformation accumulation at lower loading rates, it is granted that the *P-h* curves are right shift slightly. Above all, it can be concluded that loading rate is insensitive for as-cast BNi-2 filler metal.

For as-cast BNi-2 solder alloy, it is apparent that the unloading curve is largely elastic. In some materials, displacements recovered during initial unloading may not be entirely elastic, and because of this, the use of first unloading curves in the analysis of elastic properties can sometimes lead to inaccuracies. One way to minimize non-elastic effects is to include peak load hold periods in the loading sequence to allow time dependent plastic effects to diminish [10]. The procedure adopted to minimize effects in this study is to load and unload the indentation twice and include 10s holding periods at peak load. In addition, as shown in Fig 2 (c), at the loading rate of 1mN/s, loading curves of the as-cast BNi-2 filler alloy under different peak loads can be accurately fitted by one curve due to their overlapping characters. The unloading curves are shifted according to their final depths, they show the similar behaviour. As a result, we can say that the as-cast BNi-2 solder alloy has identical elastic and plastic deformation mechanisms throughout the entire load range [33].

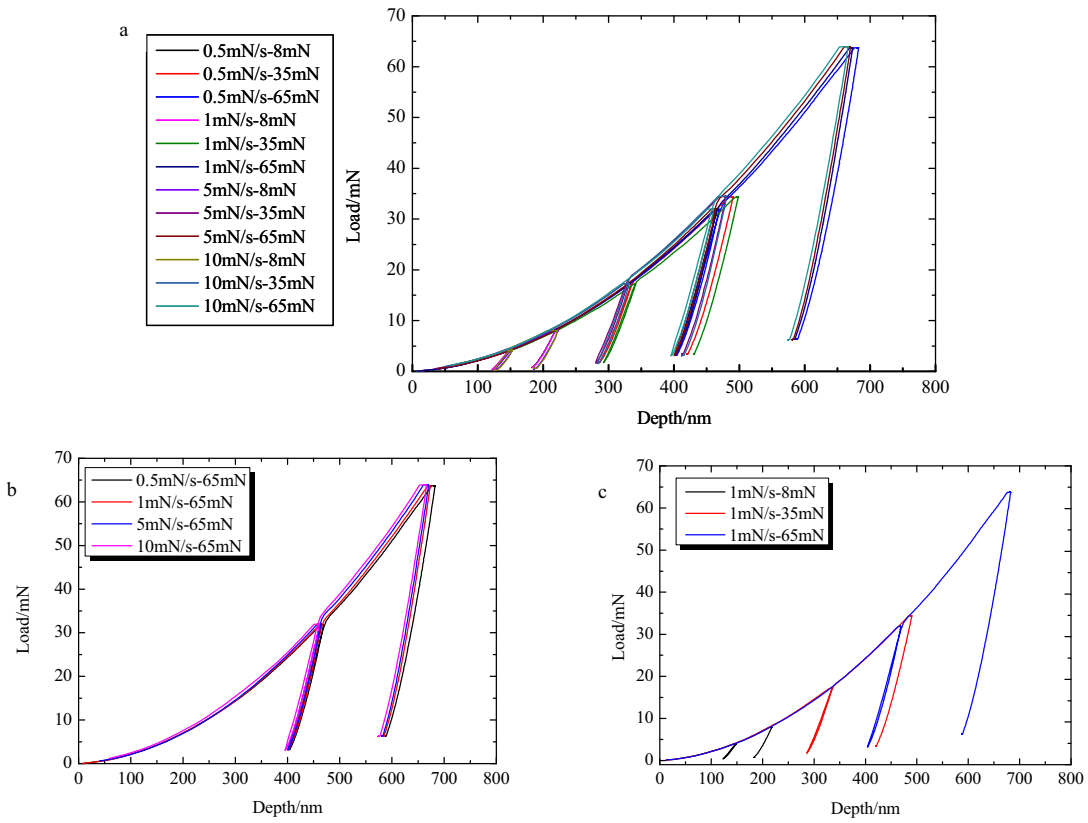

Fig. 2. Nanoindentation load displacement curves for as cast BNi-2 brazing alloy: (a) Indentation tests conducted to different conditions; (b) Influences of loading rates on load-displacement; (c) Load-displacement measured at different maximum loads.

The resulting values of modulus are plotted as a function of penetration depths as shown in Fig. 3. Young's modulus is by averaging the nanoindentation experimental results and compared with commonly accepted values from the literature. Fig. 3 also shows that the modulus with the penetration depths increasing. The average modulus value of 262.0Gpa has been gotten. The reported result on the Young's modulus of BNi-2 is around 205.1GPa [34] which has same order of magnitude to our consequence. However, the possible reasons for this disagreement may be in several aspects due to the differences of measuring techniques. Firstly, the measurement is local and can be influenced by local defects such as voids, inclusions, and crystalline defects. Whereas these allow insights into the microscopic behavior, sufficient statistics are required to obtain a meaningful value. Secondly, the indentation depths are small; the surface state (roughness, presence of oxide, friction effects) can influence the results [35]. Hence, nanoindentation is illustrated an effective method to obtain the material's properties.

The change of hardness for BNi-2 with the load is given in Fig. 4. The average hardness is 8.77GPa which calculated by Eq. (6). It is well known that indentation size effect (ISE) usually involves a decrease in the measured apparent hardness with increasing applied test load, with increasing indentation size. Investigations [36,37] have confirmed that hardness of various bulk materials were indentation size dependent especially at lower peak loads. However, in our case, hardness of as-cast BNi-2 doesn't show load dependent behavior. The load increase, results in more convergent and a little lower hardness for as-cast BNi-2 filler metal. There is very little evidence for an indentation size effect; the hardness remains more or less constant over the entire range of load. It is illustrated that the hardness is independent of indentation size effect because of a scatter distribution of the hardness.

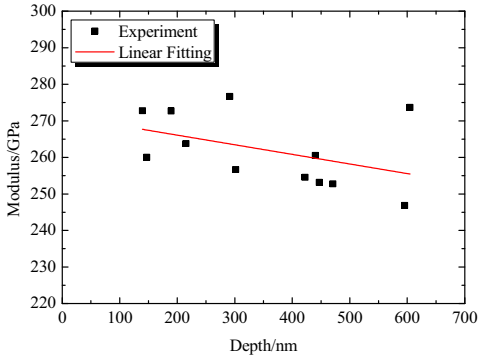

Fig. 3. Young's modulus as a function of depth into the sample measured by nanoindentation.

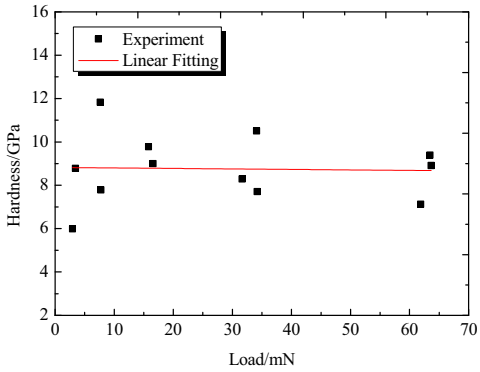

Fig. 4. Hardness as a function of the load for as-cast BNi-2 solder alloy.

3.2. Yield strength and work hardening exponent

The Young's modulus and hardness of as-cast BNi-2 filler metal, measured by nanoindentation experiments, have been reported above. The plastic properties of BNi-2 filler metal, such as yield strength and work hardening exponent, are not well known. Some recent studies have proposed models for extracting these properties of a material from the indentation load–displacement curves [21-24].

Plastic behaviour of many pure and alloyed engineering metals can be closely approximated by a power law description, as shown schematically in Fig. 5. A simple elasto-plastic, true stress–true strain behavior is assumed to be:

$$\sigma = \begin{cases} E\varepsilon, \ for\ \sigma \le \sigma_y \\ R\varepsilon^n, \ for\ \sigma \ge \sigma_y \end{cases} \tag{7}$$

where E is the Young's modulus, R a strength coefficient, n the strain hardening exponent and σ_y the initial yield stress at zero offset strain. In the plastic region, true strain can be further decomposed to strain at yield and true plastic strain, which is written as $\varepsilon = \varepsilon_y + \varepsilon_p$. For continuity at yielding, thus

$$\sigma_y = E\varepsilon_y = R\varepsilon_y^{\,n} \tag{8}$$

when $\sigma > \sigma_y$, Eqs.(7)and(8)yield

$$\sigma = \sigma_y \left(1 + \frac{E}{\sigma_y}\sigma_y \right)^n \tag{9}$$

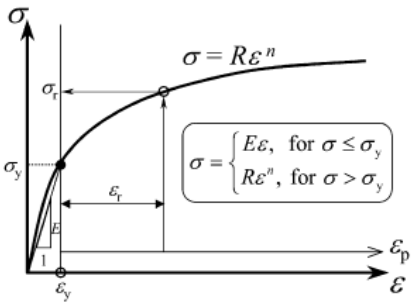

Fig. 5. The power law elasto-plastic stress–strain behavior used in the current study.

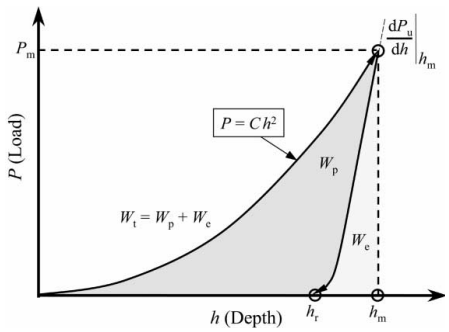

Fig. 6. Schematic illustration of a typical *P-h* response of an elasto-plastic material to instrumented sharp indentation.

With the above assumptions and definitions, a material's elasto-plastic behavior is fully determined by the parameters E, v, σ_y and n [31]. While the Young's modulus and hardness of cast filler metal BNi-2 measured by nanoindentation experiment, the plastic properties of BNi-2, such as yield strength and work hardening exponent, are not well known. Some recent studies have proposed methodologies for plastic properties prediction by making use of complex functions of the strain-hardening exponent based on nanoindentation data [10-12]. In this study, an approach is used which proposed by Dao et al. [30].

A_m is the true projected contact area measured at the maximum load P_{max} and can be identified with the hardness of the indented material. The maximum indentation on depth h_m occurs at P_{max}, and the initial unloading slope is defined as $\left.\frac{dP}{dh}\right|_{h_m}$. The W_t term is the total work done by load P during loading, W_e is the released (elastic) work during unloading and the stored (plastic) work $W_p=W_t-W_e$. The residual indentation depth after complete unloading is h_r.

Fig. 6 shows the typical *P-h* response of an elasto-plastic material to sharp indentation. During loading the response can be described by Kick's law.

$$P = Ch^2 \tag{10}$$

where P is the indentation load, h is the indentation depth, C is the loading curvature can be given by [10]

$$C = \sigma_{0.033}\Pi_1\left(\frac{E^*}{\sigma_{0.033}}\right) \tag{11}$$

where $\sigma_{0.033}$ is the representative stress at a plastic strain of 0.033 determined by the geometry of indenter [11], Π_1 is a dimensionless function, and E^* is the reduced Young's modulus. The relationship between representative stress and yield stress is then given by [10]

$$\frac{1}{E \cdot h_m}\frac{dP}{dh}\Big|_{h_m} = \Pi_2\left(\frac{E^*}{\sigma_{0.033}}, n\right) \tag{12}$$

where h_m is the maximum indentation depth, $\frac{dP}{dh}\Big|_{h_m}$ is the slope of unloading, and Π_2 is a dimensionless function.

The approaches to extract yield strength σ_y and work hardening exponent n are mostly based on the characteristic parameters of a *P-h* curve, namely C, $\frac{dP}{dh}\Big|_{h_m}$ and h_r/h_m.

The analysis procedure used to calculate the yield strength and work hardening exponent in this study are shown in Fig. 7. In order to calculate these two values conveniently, the matlab software was used.

Table 2 lists the parameters obtained from the load-displacement curves. These are essential parameters to calculate the yield strength and work hardening exponent using dimensional analysis proposed by Dao et al. [30]. Table 3 lists the mechanical property results acquired from the nanoindentation tests and analysis from Dao's model.

Table 2. Parameters obtained from load-displacement curve for dimensional analysis.

Material	C(GPa)	$\frac{dP}{dh}\Big\|_{h_m}$ (kN/mm)	$\frac{W_p}{W_t}$	$\frac{h_r}{h_m}$
As-cast BNi-2	158.636	711.28×10^3	0.7585	0.8559

Table 3. Mechanical properties obtained from nanoindentation tests and Dao's model.

Material	E (GPa)	v	E^* (GPa)	σ_y (MPa)	$\sigma_{0.033}$ (MPa)	n	H (MPa)
As-cast BNi-2	262.0	0.3	309.5	306±5	2.0965	0.57	8.77

4. Conclusions

In this study, nanoindentation tests were performed to obtain the parameters of as-cast BNi-2 filler metal elasto-plastic properties. The key results of this research can be summarized as follows:

(1) Nanoindentation load-displacement responses for as-cast BNi-2 were obtained. The filler metal has identical elastic and plastic deformation mechanisms throughout the entire load range. It is found that as-cast BNi-2 is loading rate insensitive through the analysis of the loading conditions.

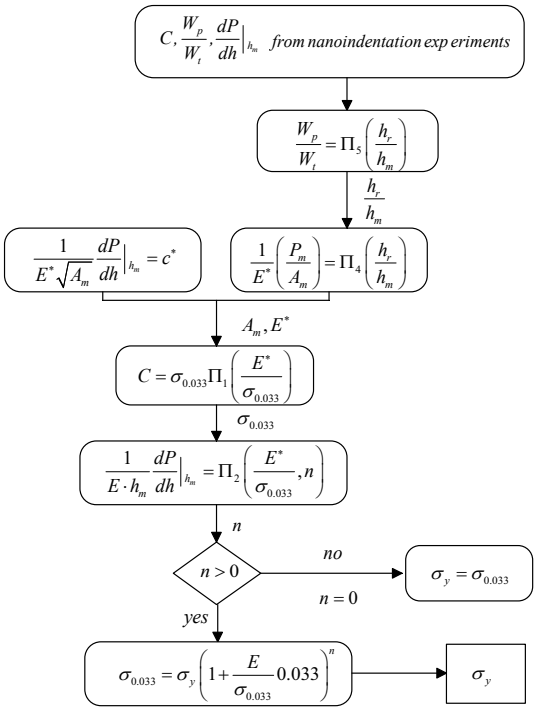

Fig. 7. Procedure for extracting work hardening exponent and yield strength using Dao's model.

(2) Young's modulus and hardness were measured by nanoindentation experiments. The Young's modulus has been obtained which has the same order of magnitude to limited data available in the literature. It is confirmed that nanoindentation is an effective method to investigate the mechanical properties of materials. The hardness remains more or less constant over the entire range of load shows that the hardness is independent of indentation size effect.

(3) The yield strength and work hardening exponent were extracted from the loading/unloading curves, using Dao's model.

Acknowledgements

This research was sponsored by Shanghai Pujiang Program (No. 14PJD015).

References

[1] Z.J. Chen, M. Wang, L.L. Feng. Effect of brazing clearance on microstructure and strength of welded joint of 316L stainless steel [J]. Advanced Materials Research; 2012, 399-401: 1890-1893.

[2] X.W. Wu, R.S. Chandel, H.P. Seow. Wide gap brazing of stainless steel to nickel-based superalloy [J]. Materials of Processing Techonology; 2001, 113: 215-221.

[3] W.C. Jiang, J.M. Gong, S.T. Tu. Effect of holding time on vacuum brazing for a stainless plate-fin structure [J]. Materials and Design; 2010, 31: 2157-2162.

[4] Y. H. Yu, M. O. Lai. Effect of gap filler and brazing temperature on fracture and fatigue of wide-gap brazed joints [J]. Materials Science; 1995, 30: 2101-2107.

[5] J. Zhang, T.P. Wang, C.F. Liu, Y.M. He. Effect of brazing temperature on microstructure and mechanical properties of graphite/copper joints [J]. Materials Science & Engineering A. 2014, 594: 26-31.

[6] J. Ruiz-Vargas, N. Siredey-Schwaller, N. Gey, P. Bocher, A. Hazotten. Microstructure development during isothermal brazing of Ni/BNi-2

couples. [J] Journal of Materials Processing Technology. 2013, 213: 20-29.
[7] H.Chen, J. M. Gong, L.Y. Geng, S. T. Tu. Numerical Analysis of thermal Deformation and Residual Stress for the Brazed Plate-Fin Structure. Proceedings of 2006 ASME Pressure Vessels and Piping Division Conference—ASME PVP2006/ICPVT-11 Conference, Vancouver, BC, Canada, Jul. 23–27
[8] B.N. Lucas, W.C. Oliver. Indentation power-law creep of high-purity indium. [J] Metal lurgical and Materials Transactions A. 1999, 30 : 601–610.
[9] C.Z. Liu, J. Chen. Nanoindentation of lead-free solders in microelectronic packaging [J]. Materials Science and Engineering A, 2007, 448: 340-344.
[10] W. C. Oliver, G. M. Pharr. An improved technique for determining hardness and elastic modulus using load and displacement sensing indentation experiments. [J]. Materials Research Innovations. 1992, 7: 1564
[11] M. F. Doener, and W. D. Nix, A method for interpreting the data from depth-sensing indentation instruments. [J] Journal of Materials Research. 1986, 1: 601.
[12] J Mencik, D Munz, E Quandt, E. R. Weppelmann. Determination of Young's modulus by spherical indentation. [J] Journal of Materials Research. 1997, 12: 2475.
[13] W. C. Oliver, C. J. Mchargue. The Hardness and Elastic Modulus of TiN Films as Determined by Ultra-Low Load Indentation. [J] MRS Online Proceedings Library. 1990, 180.
[14] R Saha, W. D. Nix. Effects of the substrate on the determination of thin film mechanical properties by nanoindentation . [J] Acta Materialia. 2002, 50: 23.
[15] J. B. Pethica, W. C. Oliver. Thin films: stresses and mechanical properties. [J] Materials Research Society Symposium Proceedings. 1989, 130: 13.
[16] H Rhee, J. P. Lucas, K. N. Subramanian. Micromechanical characterization of thermomechanically fatigued lead-free solder joints. [J] Materials Science. 2002, 13: 477.
[17] X Deng, M Koopman, N Chawla, K. K. Chawla. Measurement and prediction of Young's modulus of a Pb-free solder [J] Materials Science. 2004, 15: 385-388.
[18] R. R. Chromik, R. P. Vinci, S. L. Allen, M. R..Notis. Nanoindentation measurements on Cu-Sn and Ag-Sn intermetallics formed in Pb-free solder joints. [J] Materials Research. 2003, 18: 2251.
[19] N. J. Briot, K. Tobias, E. Christoph, and T. John Balk. Mechanical properties of bulk single crystalline nanoporous gold investigated by millimetre-scale tension and compression testing. [J] Philosophical Magazine. 2014, 94: 847-866.
[20] D. R. Frear. et al. editors. Intermetallic growth and mechanical behavior of low and high melting temperature solder alloys. [J] Metallurgical and Materials Transactions A. 1994, 25.
[21] M. Dao, N. Chollacoop, K. J. Van Vliet, T. A. Venkatesh, S. Suresh. Some critical experiments on the strain-rate sensitivity of nanocrystalline nickel. [J] Acta Materials. 2003, 51: 35159-5172.
[22] N. Chollacoop, K. S. Kumar. High-temperature compression behavior of Mo-Si-B alloys. [J] Acta Materials. 2004, 52: 5571-5587.
[23] T.A. Venkatesh, K. J. Van Vliet, A. E. Giannakopoulos, S. Suresh. An experimental investigation of fretting fatigue in Ti-6Al-4V: the role of contact conditions and microstructure. [J] Scripta Materialia. 2000, 42: 833.
[24] A. E. Giannakopoulos, S. Suresh. Continuous measurements of load-penetration curves with spherical microindenters and the estimation of mechanical properties. [J] Journal of Materials Research. 1998, 13: 1390-1400.
[25] J. L. Louber, B. N. Lucas, W. C. Oliver. NIST Special Publication 896: International Workshop on Instrumented Indentation; 1995, 31.
[26] B. N. Lucas, C. T. Rosenmayer, W. C. Oliver. Thin films: stresses and mechanical properties VII. MRS Sympos Proc 1998, 505: 97.
[27] B. N. Lucas, W. C. Oliver, J. L. Loubet, G. M. Pharr. Thin films: stresses and mechanical properties VI. Materials Research Society Symposium Proceedings. 1997, 436: 233.
[28] G. M. Pharr, D. S. Harding, W. C. Oliver. Mechanical properties and deformation behavior of materials having ultra-fine microstructures. [J] Dordrecht: Kluwer Academic Publishers; 1993, 449.
[29] D. S. Harding, W. C. Oliver, G. M. Pharr. Thin films: stresses and mechanical properties V. [J] Materials Research Society Symposium Proceedings.1995, 356: 663.
[30] M. Dao, N. Chollacoop, K. J. Van Vliet, T. A. Venkatesh, S. Suresh. Computational modeling of the forward and reverse problems in instrumented sharp indentation. [J] Acta Materials. 2001, 49: 3899-3918.
[31] X. Deng, N. Chawla, K.K. Chawla, M. Koopman. Deformation behavior of (Cu, Ag) Sn intermetallic by nanoindentaion [J]. Acta Materialia; 2004, 52 : 4291–4303
[32] G. Simmons, H. Wang. Single crystal elastic constants and calculated aggregate propeties: a handbook. Cambridge, MA: MIT Press; 1971.
[33] A.E. Ozmetin, O. Sahin, E. Ongun, M. Kuru. Mechanical characterization of MgB2 thin films using nanoindentation technique. [J] Journal of Alloys and Compounds. 2015, 619: 262-266.
[34] W.C. Jiang, J.M. Gong, H. Chen, S. T. Tu. Finite element analysis of the effect of brazed residual stress on creep for stainless steel plate-fin structure [J]. Pressrue vessel technology. 2008, 130.
[35] Y. Rosenthal, A. Stern, S.R. Cohen, D. Eliezer. Nanoindentation measurements and mechanical testing of as-soldered and aged Sn–0.7 Cu lead-free miniature joints. [J] Materials Science and Engineering A. 2010, 527: 4014–4020.
[36] O. Uzun, T. Karaaslan, M. Gogebakan, M. Keskin. Hardness and microstructural characteristics of rapidly solidified Al-8-16 wt.%Si alloys. [J] Journal of Alloys and Compounds. 2004, 376: 149-157.
[37] U. Kölemen, O. Uzuna, M.A. Aksan, N. Güçlü E. Yakıncı. An analysis of load-depth data in depth-sensing microindentation experiments for intermetallic MgB_2. [J] Journal of Alloys and Compounds. 2006, 415: 294-299.